Chapter 19

Multi-Mode Interference Devices

XAVEER LEIJTENS AND MEINT SMIT

19.1 Introduction

waveguide coupler
power splitter
power combiner

Waveguide couplers can be used for coupling light between two or more waveguides, for splitting power from one to a number of waveguides (power splitter) or combining light from a number of waveguides into a single waveguide (power combiner). Figure 19.1 shows a number of different couplers. Couplers a, b and c are $1 \times N$ couplers. Couplers d, e and f are $M \times N$ couplers, they couple light from multiple input ports to multiple output ports.

Self Imaging
Multi-Mode Interference
MMI

We can distinguish between different types of couplers: branching (Y-junctions), radiation couplers, evanescent wave couplers, and couplers based on Self Imaging. The latter are usually called Multi-Mode Interference (MMI) devices. They are used most frequently in high-contrast waveguide systems, like in semiconductor-based PICs. They have the advantage that they are compact, but at their interfaces with the input and output waveguides they experience loss and reflections. By proper design the loss can be minimized below a few tenths of a dB and the reflection below −30 dB.

MMI-devices are composite building blocks: they consist of a multimode waveguide section and two junctions with other waveguides at both sides of the multimode waveguide. In this chapter we describe the MMI-couplers and a few other devices which are based on Multi-Mode Interference, such as filters and reflectors. The other couplers are described in following chapters.

19.2 Multi-Mode Interference (MMI) and Self Imaging

Figure 19.2 shows a simulated intensity pattern in a multi-mode waveguide section and the corresponding experimentally imaged pattern. At the left side light is coupled into the device from a narrow single-mode waveguide. In the wide section the light is no longer laterally confined and starts to diffract into a divergent beam. After propagating some distance it is reflected by the side walls and starts interfering with itself, which gives rise to a fascinating interference pattern. At the right hand side of the wide waveguide section all the light focuses in two spots: a double image of the input beam. At two thirds of the imaged length the input beam appears to image in three spots.

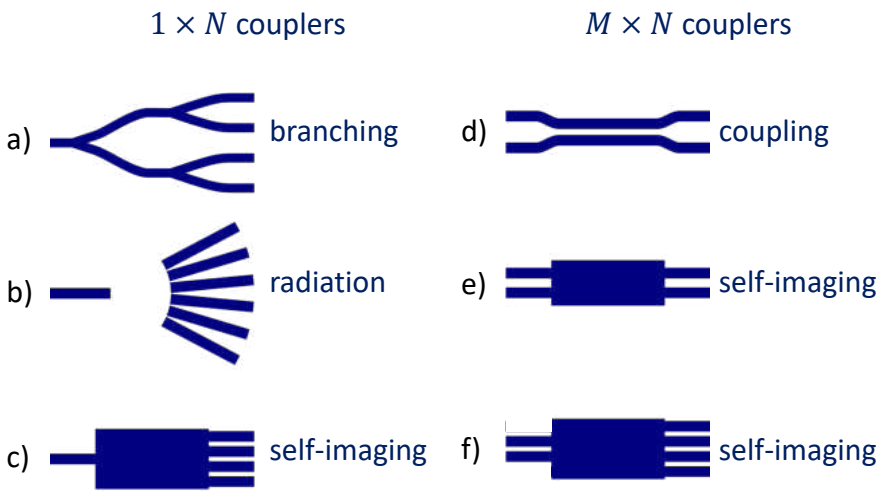

Figure 19.1: Different coupler types.

Halfway we observe four images and a bit before that five and even six images. The experimentally imaged pattern shows how good the experimental results agree with the simulation.[1]

If we connect two output waveguides at the end, as shown in Fig. 19.2d, we have a 1×2 power splitter. If we cut the waveguide at half of its length, as shown in Fig. 19.2c, and connect four output waveguides, we have a 1×4 splitter.

In the following paragraphs we will give an explanation of the self-imaging properties of multi-mode waveguides and discuss a number of applications.

19.3 Analysis of the imaging mechanism

imaging

To analyze the imaging properties of a multimode waveguide section we decompose the exciting field $U(y,0)$ at the input junction of the waveguide into its modal components, propagate them through the waveguide and reconstruct the field at the end of the waveguide as the sum of the modes.

The field $U(y,0)$ at the input can be described as:

$$U(y,0) = \sum a_i U_i(y) \tag{19.1}$$

in which $U_i(y)$ is the field of mode i and a_i is its excitation coefficient. The field $U(y,L)$ at length L follows as:

$$U(y,L) = \sum a_i U_i(y) \cdot e^{-j\beta_i L} \tag{19.2}$$

[1] The experimental image has been measured in an Al_2O_3 waveguide, which was heavily doped with Erbium atoms [168]. In such a highly doped waveguide coupled Erbium atoms can absorb the energy of a number of infrared photons (1550 nm) and emit it as green light (upconversion). The green light is emitted in all directions and it is proportional to (the fourth power of) the IR-intensity. By making a photograph of the green light pattern as seen through a microscope above the wafer we get an image of the IR intensity pattern in the waveguide, but imaged with green light. Because the wavelength of green light is three times shorter than the IR wavelength, we can image the IR light pattern with a resolution far below the diffraction limit of IR-light. A simple microscope is, therefore, sufficient to make a high-resolution image of the IR intensity pattern as shown in Fig. 19.2.

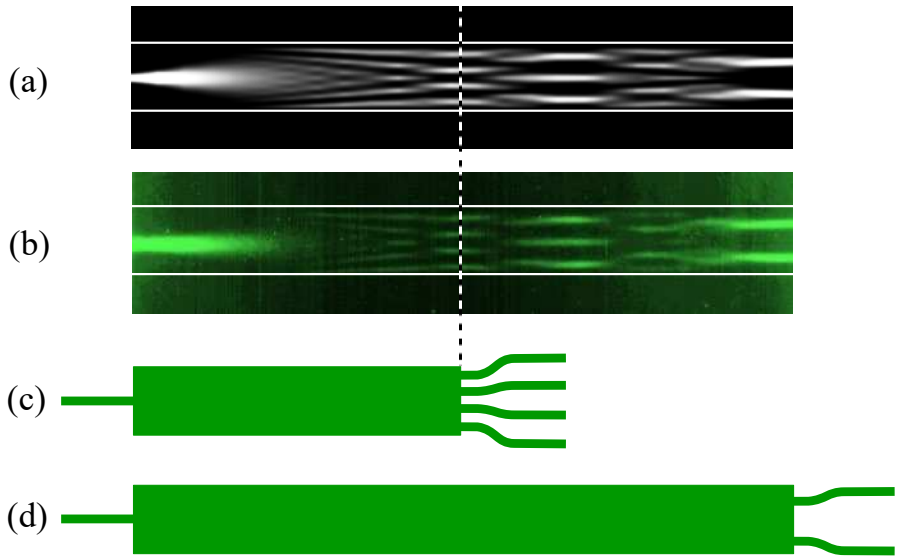

Figure 19.2: Multimode Interference
a) simulated intensity pattern
b) experimentally imaged pattern.
c) layout of a 1 × 4 coupler
d) layout of a 1 × 2 coupler

in which β_i is the propagation constant of mode i. The shape of $U(y,L)$ is only dependent on the phase difference between the modes, so we can take the phase factor $e^{-j\beta_0 L}$ of the fundamental mode out of the summation. We then find

$$U(y,L) \quad = \quad \sum a_i U_i(y) \cdot e^{-j(\beta_i-\beta_0)L} = \sum a_i U_i(y) \cdot e^{j\Delta\beta_{0i}L} \tag{19.3}$$

in which

$$\Delta\beta_{0i} = \beta_0 - \beta_i \tag{19.4}$$

If the phase difference $\Delta\beta_{0i}L$ of all the modes with the fundamental mode equals a multiple of 2π, then the field at that length will be an image of the input field, which explains the name self imaging which is sometimes used for Multi-Mode Interference. The lengths at which this self-imaging occurs can be found by analyzing the relation between the longitudinal and the transverse propagation constants. Figure 19.3 illustrates their dependence. In strongly multimoded waveguides the lower order modes will be almost completely confined so that their lateral mode profiles will contain an integer number of half periods within the waveguide. Therefore, the higher-order mode profiles are spatial harmonics of the fundamental mode profile and their transverse propagation constants k_{yi} will be integer multiples of the fundamental one (see Chapter 2, Sec. 2.2.2):

self imaging
Multi-Mode Interference

transverse propagation constant

$$\begin{array}{rcl} k_{yi} & \approxeq & (m+1)k_{y0} \\ k_{y0} & \approxeq & \frac{\pi}{W} \end{array} \tag{19.5}$$

in which m is the number of the mode and W is the width of the multimode waveguide section. The corresponding propagation constant β_i follows as:

$$\beta_m = \sqrt{N_1^2 k_0^2 - k_{ym}^2} \approxeq N_1 k_0 - \frac{1}{2}(m+1)^2 \frac{k_{y0}^2}{N_1 k_0} \tag{19.6}$$

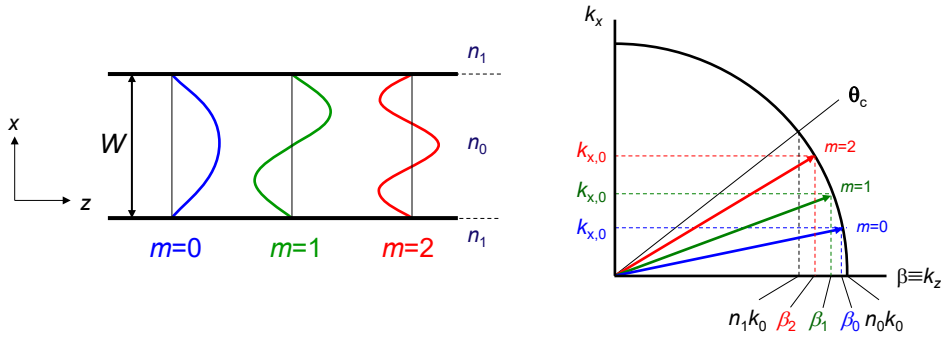

Figure 19.3: The relation between the transverse and the longitudinalpropagation constant in a strongly multimoded waveguide.

effective index

in which N_1 is the effective index in the waveguide region (see Sec. 2.5.1 of Chapter 2 and k_0 is the wavenumber in vacuum. By substituting $\beta_0 \approxeq N_1 k_0 - \frac{1}{2}\frac{k_{y0}^2}{N_1 k_0}$ we find:

$$\Delta\beta_{0m} = \beta_0 - \beta_m = \frac{1}{2}m(m+2)\frac{k_{y0}^2}{N_1 k_0} = \frac{m(m+2)}{3}\Delta\beta_{01} \tag{19.7}$$

in which

$$\Delta\beta_{01} = \frac{3\pi}{2N_1 k_0 W^2}. \tag{19.8}$$

The length L_π over which the fundamental and the first order mode get π phase difference is related to $\Delta\beta_{01}$ according to:

$$L_\pi = \frac{\pi}{\Delta\beta_{01}} \tag{19.9}$$

At length L the phase Φ_m of the modes is

$$\Phi_m = \beta_m L \tag{19.10}$$

and their phase difference $\Delta\Phi_{0m}$with the fundamental mode is

$$\Delta\Phi_{0m}(L) = (\beta_0 - \beta_m)L = \frac{m(m+2)}{3}\pi\frac{L}{L_\pi} \tag{19.11}$$

19.3.1 Full image

From Eq. 19.11 we see that for a length $L = 6L_\pi$ the phase difference between the modes follows from

$$\Delta\Phi_{0m}(6L_\pi) = (\beta_0 - \beta_m)\cdot 6L_\pi = m(m+2)\cdot 2\pi$$

self-imaging length

Table 19.1 row (b) shows the values of $m(m+2)$ for the different modes. For the self-imaging length $L_{si} = 6L_\pi$ all modes have zero relative phase, apart from a multiple of 2π, as shown in Table 19.1, row (e), so that they will reproduce an image of the input field, as depicted in Fig. 19.4.

a		m	0	1	2	3	4	5	6	7	8	9	...
b	General	$m(m+2)$	0	3	8	15	24	35	48	63	80	99	...
c	Symmetric	$\frac{m(m+2)}{8}$	0	-	1	-	3	-	6	-	10	-	...
d	Paired	$\frac{m(m+2)}{3}$	0	1	-	5	8	-	16	21	-	33	...
e	$L_{si} = 6L_\pi$	$\mod\{\Delta\Phi_{0i,si}, 2\pi\}$	0	0	0	0	0	0	0	0	0	0	...
f	$L_{mi} = 3L_\pi$	$\mod\{\Delta\Phi_{0i,mi}, 2\pi\}$	0	π	0	π	0	π	0	π	0	π	...
g	$L_{3dB} = \frac{3}{2}L_\pi$	$\mod\{\Delta\Phi_{0i,3dB}, 2\pi\}$	0	$\frac{3\pi}{2}$	0	$\frac{3\pi}{2}$	0	$\frac{3\pi}{2}$	0	$\frac{3\pi}{2}$	0	$\frac{3\pi}{2}$	...

Table 19.1: The relative phase of the modes in an MMI-coupler for different lengths of the MMI-section and different excitation conditions.

19.3.2 Mirrored Image

At half the self-imaging length $L = 3L_\pi$ the relative phase difference $\Delta\Phi_i = m(m+2)\cdot\pi$. We see that for even modes $m(m+2)$ is even, so $\Delta\Phi_{0m}$ will be zero, apart from a multiple of 2π.,so all even modes have the same phase. For odd modes $m(m+2)$ is odd, so $\Delta\Phi_{0m}$ will equal π, apart from a multiple of 2π, as shown in row (f) of Table 19.1. If we separate the input field in an even and an odd part:

$$U(y,0) = U_{even}(y,0) + U_{odd}(y,0) \tag{19.12}$$

we find

$$\begin{aligned} U(y,L) &= U_{even}(y,0)e^{j\Delta\Phi_{even}} + U_{odd}(y,0)e^{j\Delta\Phi_{odd}} \\ &= U_{even}(y,0) - U_{odd}(y,0) = U_{even}(-y,0) + U_{odd}(-y,0) \\ &= U(-y,L) \end{aligned} \tag{19.13}$$

So we see that at a length

$$L_{mi} = \frac{1}{2}L_{si} = 3L_\pi \tag{19.14}$$

a mirrored image occurs, as shown in Fig. 19.4. Obviously a coupler with length L_{si} acts as a coupler in the bar state, whilst a coupler with length L_{mi} works as a cross coupler. By comparing with classical directional couplers (see Chapter 2, Eq. 2.96) we see that $L_{mi} = 3L_c$, in which $L_c = \pi/\Delta\beta_{01}$is the length of a classical cross coupler. Now it looks as if the classical directional cross coupler is shorter. This is not true, however, because in an MMI-coupler $\Delta\beta_{01}$ is significantly larger than in evanescently coupled waveguides.

mirrored image

19.3.3 3-dB coupler

Also MMI-couplers with a length $\frac{3}{2}L_\pi$ have interesting properties. From Table 19.1 row (g) we see that the even modes have zero phase difference and the odd modes $\frac{3\pi}{2}$. So for the field U(y, L=$\frac{3}{2}L_\pi$) we find after some manipulation (see Problem 19.1):

$$U(y, \tfrac{3}{2}L_{2\pi}) = \tfrac{1}{2}\sqrt{2}\{U(y,0) + jU(-y,0)\} \tag{19.15}$$

From this formula we see that at a length $\frac{3}{2}L_{2\pi}$ the signal power is equally distributed over the direct image $U(y,0)$ and the mirrored image $U(-y,0)$, and that there is 90° phase difference between the two. So an MMI-coupler with a length $\frac{3}{2}L_\pi$ acts as a 3-dB hybrid coupler.

3-dB hybrid coupler

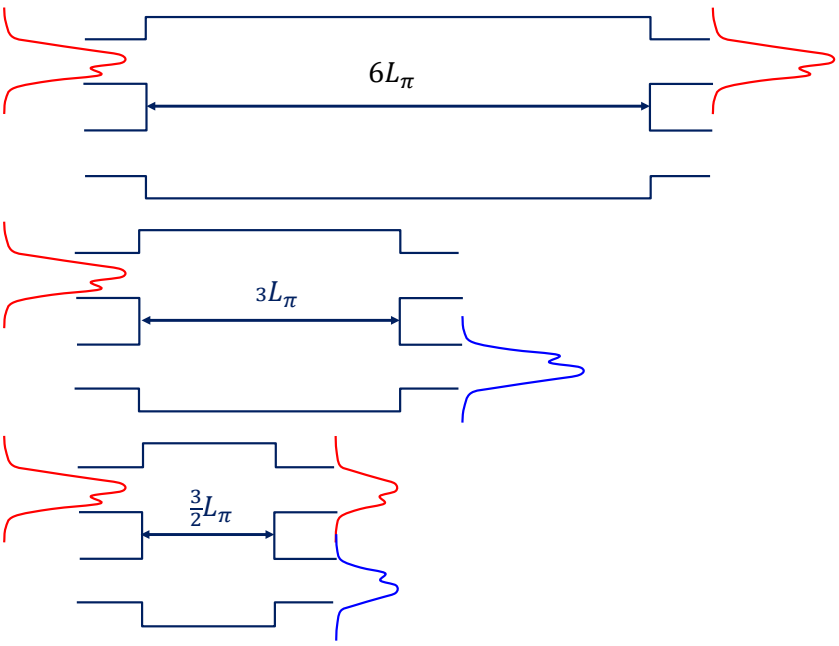

Figure 19.4: Self-imaging: bar coupler, cross coupler and 3-dB coupler.

Problem 19.1: Output signals of a 3-dB MMI-coupler.

Problem: Show that in a 2x2 MMI-coupler with length $\frac{3}{2}L_\pi$ the input signal at one port is equally divided over the two output ports, but with 90° phase difference.

Solution: By remembering that $U_{\text{odd}}(-y,0) = -U_{\text{odd}}(y,0)$ and $\frac{1}{2}\sqrt{2}(e^{-j\pi/4} + e^{j\pi/4}) = 1$ we find:

$$\begin{aligned}
U(y,\tfrac{3}{2}L_\pi) =& U_{\text{even}}(y,0) + U_{\text{odd}}(y,0)e^{j3\pi/2} \\
=& \tfrac{1}{2}\sqrt{2}\left(e^{-j\pi/4} + e^{j\pi/4}\right)\left\{U_{\text{even}}(y,0) + U_{\text{odd}}(y,0)e^{j3\pi/2}\right\} \\
=& \tfrac{1}{2}\sqrt{2}\left\{\left(e^{-j\pi/4} + e^{j\pi/4}\right)U_{\text{even}}(y,0) - \left(e^{j\pi/4} - e^{j\pi/4}\right)U_{\text{odd}}(y,0)\right\} \\
=& \tfrac{1}{2}\sqrt{2}\left\{e^{-j\pi/4}\left[U_{\text{even}}(y,0) + U_{\text{odd}}(y,0)\right]\right. \\
&\left. + e^{j\pi/4}\left[U_{\text{even}}(-y,0) + U_{\text{odd}}(-y,0)\right]\right\} \\
=& \tfrac{1}{2}\sqrt{2}e^{-j\pi/4}\left\{U(y,0) + e^{j\pi/2}U(-y,0)\right\} \\
=& \tfrac{1}{2}\sqrt{2}e^{-j\pi/4}\left\{U(y,0) + jU(-y,0)\right\}.
\end{aligned}$$

If we neglect the common phase term in the even and odd part we find:

$$U(y,\tfrac{3}{2}L_\pi) = \tfrac{1}{2}\sqrt{2}\left\{U(y,0) + jU(-y,0)\right\}.$$

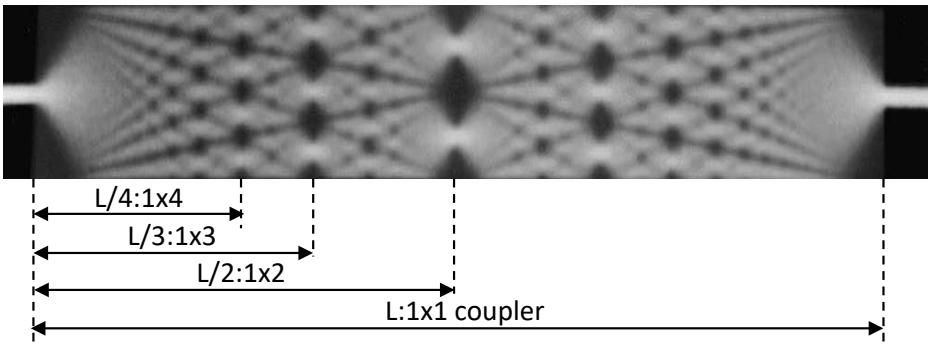

Figure 19.5: Interference pattern in a symmetrically excited coupler

19.3.4 Restricted interference: symmetric excitation

Figure 19.5 shows the interference pattern in an MMI-section which is excited in the center by a (symmetric) single-mode waveguide. We see that with such an interference pattern a 1×2 coupler has half the length of a 1×1 coupler, a 1×3 coupler has $1/3$ of the length, a 1×4 coupler $1/4$, and so on.

Symmetrically excited $1 \times N$ couplers can be much shorter than general MMI-couplers, because the odd modes are not excited and the interference pattern is formed only by even modes. The interference mechanism in such a coupler is called restricted interference. In Table 19.1 row (b) we see that for all even modes $m(m+2)$ is a multiple of 8. This means that we get full imaging already at a length

restricted interference

$$L_{si,symm} = 6L_\pi/8 \tag{19.16}$$

and the length of a symmetric 1xN-coupler is shortened to

$$L_{1xN,symm} = 6L_\pi/8N \tag{19.17}$$

as shown in row (g) from Table 19.1.

19.3.5 Restricted interference: paired interference

An interesting case occurs when we excite the MMI-section with waveguides positioned at $1/3$ and $2/3$ of the MMI-section width (i.e. at $y = \pm\frac{1}{6}W$). From Fig. 19.6 we see that if the excitation is symmetric around the dashed lines the modes $2,5,8,\ldots$ will not be excited because they are anti-symmetric around these lines. So the interference pattern will be formed by modes 0 and 1, 3 and 4, 6 and 7, and so on. That's why this case is called paired interference.

From row (d) in Table 19.1 we see that for these paired modes $m(m+2)$ is a multiple of 3, so a paired-interference coupler can be designed three times shorter than the general self-imaging coupler:

$$L_{si,pi} = L_{si}/3 \tag{19.18}$$

For an optimal design we have to use the effective width W_e rather than the physical width W of the MMI-section (see Chapter 2, Eq. 2.29). Because the effective width differs for the different modes (it increases for higher order modes) full optimization of

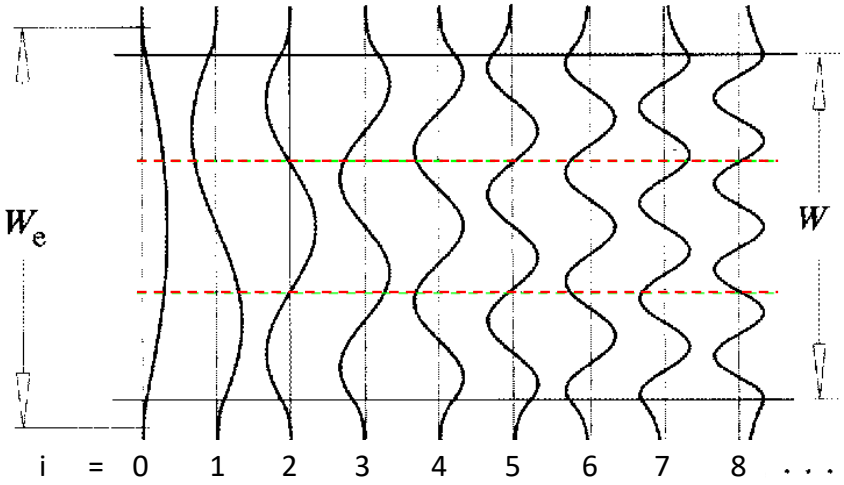

Figure 19.6: Interference pattern in a symmetrically excited coupler

Interference mechanism	General	Symmetric	Paired
Inputs x Outputs	$N \times N$	$1 \times N$	$2 \times N$
First full image	$3L_\pi$	$3L_\pi/4$	L_π
First N-fold image	$3L_\pi/N$	$3L_\pi/4N$	L_π/N
Excitation requirements	none	$a_m = 0$ for $m = 1,3,5,\ldots$	$a_m = 0$ for $m = 2,5,8,\ldots$
Input locations	any	$y = \pm W_e/6$	$y = 0$

Table 19.2: Summary of MMI-characteristics

the input waveguide positions requires numerical simulations. In high-contrast waveguides the difference with positioning the waveguide at $y = \pm\frac{1}{6}W$ will be small.

Table 19.2 gives a summary of the different MMI-couplers discussed in this chapter.

19.4 MMI-couplers

19.4.1 Optimization of access waveguide width

Figure 19.7 shows simulated interference patterns in a 2×2 coupler for different access waveguide width. For each case the same number of modes is used in the simulation of the MMI, but the excitation is different due to the difference in access waveguide width. Narrow access waveguides produce a large diffraction angle inside the MMI-section and, consequently, a small focal depth (see Chapter 2, Eq. 2.28). This is detrimental for the tolerance of the coupler. Small variations of the MMI-section width W lead to deviations of the modal propagation constants, which lead to a change in length $L_{3\text{dB}}$ at which the coupler forms its image. From the figure we see that for large waveguide widths, the divergence of the beam is small and, consequently, the depth over which the change in beam width is large, which makes the coupler less sensitive to fabrication tolerance.

focal depth

Figure 19.8 shows the schematic layout of an optimal design, including offsets at the junctions between access waveguides with different curvatures (see Chapter 10). A

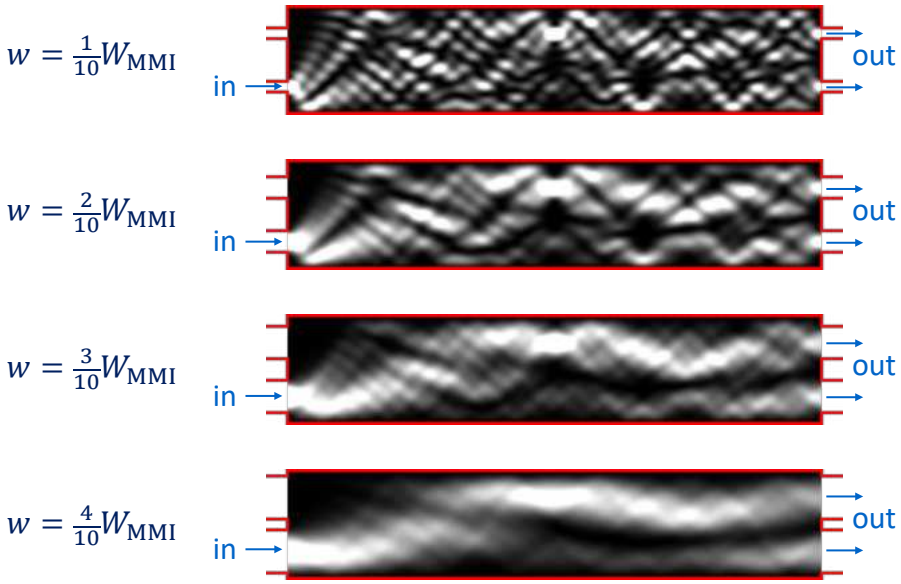

Figure 19.7: MMI intensity patterns for different access waveguide widths.

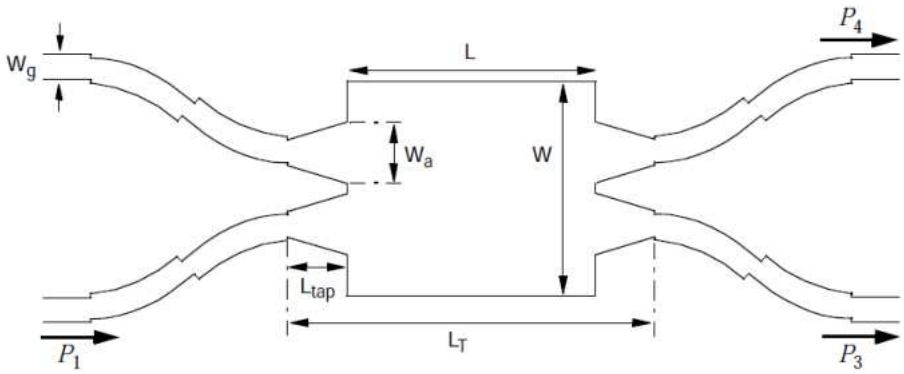

Figure 19.8: MMI intensity patterns for different access waveguide widths.

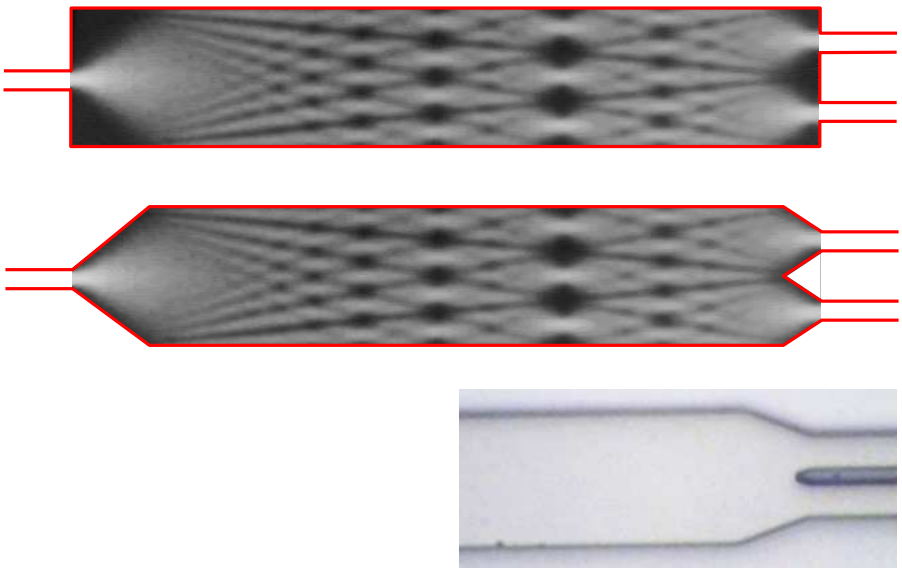

Figure 19.9: MMI-coupler with angled facets for reducing back reflections: simulations and microscope photograph [60].

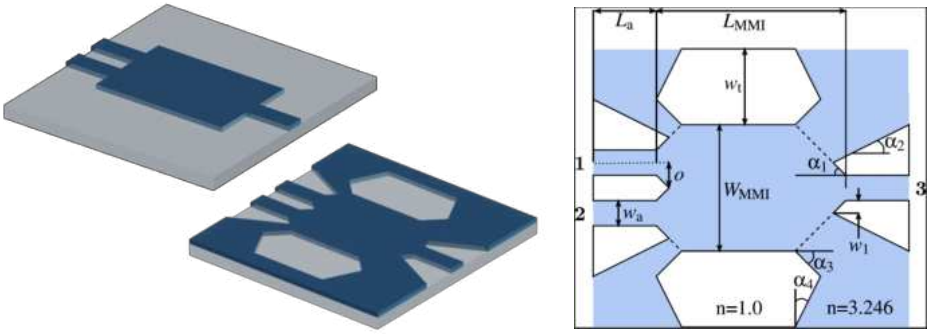

Figure 19.10: Optimized design for low reflection [169].

detailed description is given by Hill [59]. From his study a ratio $\frac{w_a}{W} = 0.3$ appears to be a good design choice.

19.4.2 Design for low reflection

A disadvantage of deep-etched MMI-couplers is that they have significant reflections at the end facets, as compared to directional couplers based on evanescent wave coupling. There a few design options for reducing these reflections.

1. We can restrict the deep etched region to the side walls of the MMI-section and apply a shallow etch at the end faces of the MMI-coupler.

2. Instead of orthogonal end faces we can tilt the end faces so that reflections are no longer directed to the input, as illustrated in Fig. 19.9. Because the light intensity at the facets is very low the effect of the angled facets on the transmission is very small. Figure 19.10illustrates an advanced design, where facets are only present

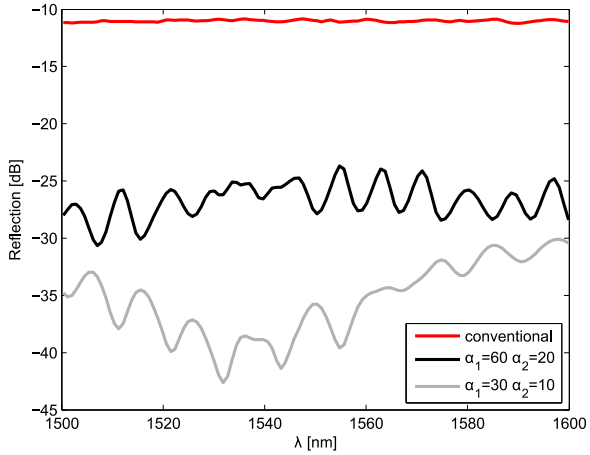

Figure 19.11: Reflection reduction for different facet angles [169].

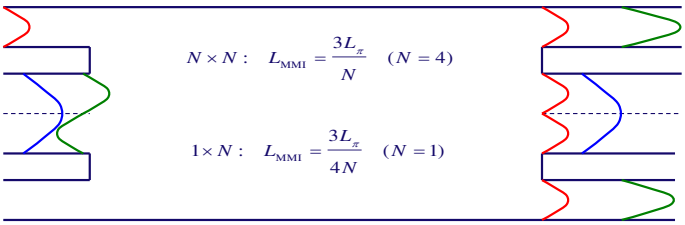

Figure 19.12: Schematic of mode-filter constructed from a 4 × 4 and 1 × 1 MMI.

where they are needed to define the waveguide edges, and are absent at positions where they are not needed for the self-imaging process. Figure 19.11 shows that an improvement of more than 20 dB is possible with a proper choice of the facet angles. Experimental results show reflection reductions well over 10 dB.

19.5 MMI-filters

Multimode interference devices can be designed to act as a mode-filter or a mode-splitter. An example is given here of an MMI that is used as a mode-filter: it passes the fundamental mode but does not pass the first-order mode. The operation principle is illustrated with figure 19.12, that shows an MMI with a different geometry of input and output waveguides. The length of the MMI can be calculated with the use of table 19.2. We consider this MMI to be either a 1×1 MMI or a 4×4 MMI. The length of the 4×4 MMI (general interference) is $3L_\pi/N$, where $N=4$ and that of the 1×1 MMI (symmetrical interference) is $3L_\pi/4N$, where $N=1$. Both result in the same length, $L_{\mathrm{MMI}}=\frac{3}{4}L_\pi$. So the same device can act differently, depending on the excitation. If we excite the MMI with a fundamental mode in the upper left waveguide (shown in red), the field will be split in 4 equal parts in the four outputs. If we excite the MMI with a fundamental mode in the (wider) central input (shown in blue), it will be imaged onto the central output. If we excite the MMI with the first-order mode in the central (wider) input (shown in green), this can be considered as exciting the MMI with a fundamental mode mode in both the 2nd and 3rd (narrow) input waveguides, with a 180° phase difference between

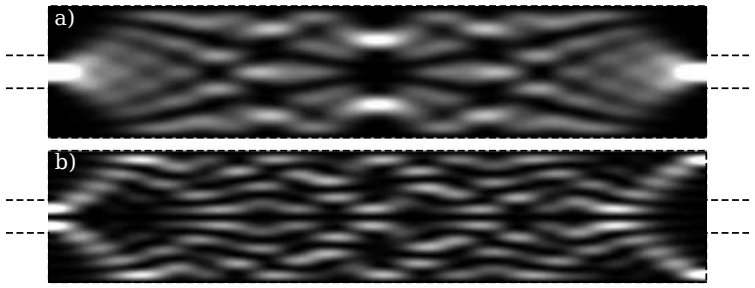

Figure 19.13: Simulated intensity pattern in MMI mode-filter, with a) fundamental mode excitation and b) first order mode excitation in the left input waveguide.

them. This will result in each of them being split in 4 equal outputs, but with opposite phase in the center two output ports, thus canceling due to destructive interference, and with equal phase in the outer outputs, thus adding constructively.

A simulation of the operation of this device is illustrated in figure 19.13, which shows the intensity pattern of the light in the MMI mode-filter when it is excited with the fundamental mode (top figure) or when it is excited with the first order mode (bottom figure). The fundamental mode is imaged onto the output waveguide, whereas the first-order mode is imaged away from the output waveguide. Clearly, the edges of the MMI have to be angled to prevent reflections, as was explained in section 19.4.2.

19.6 MMI-reflectors

[63]

19.7 Description of available PDK modules